Journal of Power Sources 255 (2014) 76–84

Contents lists available at ScienceDirect

Journal of Power Sources

journal homepage: www.elsevier.com/locate/jpowsour

Experimental identification of the active sites in pyrolyzed carbon-supported cobalt–polypyrrole–4-toluenesulfinic acid as electrocatalysts for oxygen reduction reaction

Hao-Dong Sha [a], Xianxia Yuan [a,*], Lin Li [a], Zhong Ma [a], Zi-Feng Ma [a], Lei Zhang [b], Jiujun Zhang [b]

[a] Department of Chemical Engineering, Shanghai Jiao Tong University, Shanghai 200240, China
[b] NRC Energy, Mining & Environment Portfolio, National Research Council Canada, Vancouver, BC V6T 1W5, Canada

HIGHLIGHTS

- Co–PPy–TsOH/C as electrocatalysts towards oxygen reduction reaction (ORR).
- Effects of acid leaching and second heat treatment on catalyst performance.
- Effects of cobalt loading on catalyst performance.
- The identified ORR active site in the Co–PPy–TsOH/C catalysts.

ARTICLE INFO

Article history:
Received 25 September 2013
Received in revised form
3 January 2014
Accepted 4 January 2014
Available online 10 January 2014

Keywords:
Oxygen reduction reaction (ORR)
Non-noble metal catalysts
Cobalt–polypyrrole
Acid washing
Active site

ABSTRACT

A series of carbon supported cobalt–polypyrrole–4-toluenesulfinic acid have been pyrolyzed in an argon atmosphere at 800 °C, then structurally characterized and electrochemically evaluated as oxygen reduction reaction (ORR) catalysts in aqueous 0.5 M sulfuric acid. The structures are cobalt bonded to nitrogen species (Co–N_x) along with metallic cobalt and cobalt oxide. When the cobalt loading in the compound is less than 1.0 wt%, the predominate form is Co–N_x, when the loading is higher than 1.0 wt%, metallic Co and Co oxide particles co-exist with the Co–N_x compound. At a Co loading of ~1.0 wt%, the catalyst gives the best ORR activity. Both metallic Co and Co oxide are not active for catalyzing ORR, and block the catalytically active Co–N_x species from the surface and reduce the catalytic activity since the diffusion limiting current density on a rotating disk electrode (RDE) increases when the electrode blocking agents are washed away with acid.

1. Introduction

Proton exchange membrane fuel cells (PEMFCs), as a kind of clean and high efficiency energy conversion devices, have been recognized as the potential future power sources for many applications such as the zero/low-emission vehicles, stationary and portable power stations [1,2]. However, there are still some obstacles such as high cost and insufficient durability hindering their commercialization. In overcoming these two major challenges, PEMFC electrocatalysts for cathode oxygen reduction reaction (ORR) have been identified as one of the major target materials for further development and performance improvement. At current state of technology, the platinum (Pt)-based ORR electrocatalysts seem to be the most practical in terms of both catalytic activity and stability. However, the limited supply and high cost of Pt are the barriers for the sustainable applications. Thus, reducing Pt usage or replacing Pt with non-noble metal catalysts is critical to PEMFC commercialization [3,4].

Regarding non-Pt ORR catalysts, several types of transition metal-based materials have been explored, including (1) transition metal macrocyclic compounds, [5–7] (2) carbon supported transition metal-nitrogen complexes (M–N/C compounds, normally M = Fe or Co) synthesized by pyrolysis using metal salt, carbon, and nitrogen sources as the precursors, [8–11] and (3) transition metal chalcogen compounds [12–14]. Among them, the pyrolyzed M–N/C compounds have been confirmed as the most efficient ORR catalyst in recent years due to their relatively high electrocatalytic activity, low cost and simple synthetic procedures.

* Corresponding author. Tel.: +86 21 54742827; fax: +86 21 54741297.
E-mail address: yuanxx@sjtu.edu.cn (X. Yuan).

0378-7753/$ – see front matter © 2014 Elsevier B.V. All rights reserved.
http://dx.doi.org/10.1016/j.jpowsour.2014.01.013

Although much research has been done on the pyrolyzed M–N/C catalysts, their catalytic ORR mechanisms are not yet fully understood due to the structures of precursor metal complexes can be partially destroyed during the pyrolysis process. This pyrolysis process cannot only produce M–N_x group such as M–N_2 and M–N_4 but also produce metallic and metal oxide species on the carbon particle surface. Although M–N_x groups were proposed as the ORR active sites, the contribution of metallic and metal oxide species to the ORR activity seemed not to be distinguished from that contributed by M–N_x sites [8,15,16]. Lee et al. [17] proposed that M–N_x–C ($X = 2$ or 4) could be the active sites, which might be responsible for two- and four-electron transfer ORR pathways. Some literature reported that metal-nitrogen bond would not survive during the high temperature pyrolysis but the metal and/or its oxide particles might work as the real ORR active sites in pyrolyzed M–N/C catalysts [6,9]. Normally, the central metal atom in the catalysts is believed to play a very important role [18]. Through acid washing the pyrolyzed catalysts with intention to remove metallic and metal oxide species, no significant change in the ORR performance before and after acid washing could be observed, suggesting that the metals and metal oxides themselves probably not contribute too much to ORR activity, but the actual active sites might rely on other insoluble surface species [19–21]. Some literature reported that the ORR active sites should be composed of carbon and nitrogen such as the pyridinic nitrogen (–C=N–C–) sitting on the edge planes of the carbon layer [22,23] and the graphitic-N which is bonded to three carbon atoms inside the carbon layer [24–26]. Li et al. [27] reported that the cooperative interaction (synergy) among the metal, nitrogen and carbon should be the key factor in improving the ORR kinetics. Even though the active sites for ORR in pyrolyzed M–N/C catalysts is still under discussion, some consensus have been drawn: [4,28,29] (i) the nitrogen and carbon atoms are necessary for catalytic ORR activity, and (ii) the presence of the metal atoms during the high-temperature pyrolysis of carbon supported transition metal-nitrogen complexes can contribute to the ORR enhancement catalyzed by the resulting catalysts.

As a member of M–N/C catalysts, pyrolyzed cobalt–polypyrrole (PPy)–4-toluenesulfinic acid (TsOH) supported on carbon, (Co–PPy–TsOH/C)$_P$, has demonstrated exciting ORR performance used as cathode catalyst in PEMFCs [10]. In the effort to obtaining the fundamental understanding about the catalytic active sites and their catalyzed ORR mechanisms, in this work, a series of (Co–PPy–TsOH/C)$_P$ catalysts as well as some contrastive samples were synthesized. The morphologies/structures and compositions were characterized using the powder X-ray diffraction (XRD), the transmission electron microscopy (TEM) images, X-ray photoelectron spectroscopy (XPS) and inductively coupled plasma (ICP) spectrometric measurements. The catalytic ORR activities of the synthesized catalysts were examined using cyclic voltammetry (CV) and rotating disk electrode (RDE) experiments. Furthermore, the morphology/structure–performance relationship has been discussed to distinguish the catalytic active sites and the role of each element in the catalysts.

2. Experimental section

2.1. Catalysts synthesis

In synthesizing the precursor for the pyrolyzed catalyst of (Co–PPy–TsOH/C)$_P$, a carbon suspension was first prepared by adding 0.6 g of BP2000 carbon powder (Cabot, USA, pretreated with 6 M HNO_3) to 100 ml of isopropyl alcohol under ultrasonication for 1 h at room temperature. Then, 3 mmol of freshly distilled pyrrole and 100 ml of double distilled (DI) water were added into this carbon suspension under stirring for 30 min to form a mixture. After that, 100 ml of 0.06 mol l^{-1} ammonium peroxydisulfate (APS) aqueous solution as oxidant and 0.1902 g of TsOH as additive were introduced into this mixture, followed by an additional vigorous stirring for 4 h. The resulted mixture solution was then filtered, washed and dried at 45 °C for 12 h to obtain the PPy–TsOH impregnated carbon powder material (PPy–TsOH/C). Then, 0.5 g of this PPy-TsOH/C and 0.2 g of $Co(Ac)_2 \cdot 4H_2O$ were mixed together with 200 ml of DI water. The formed mixture was ultrasonically mixed for 1 h and another vigorous stirring for 2 h, followed by an evaporation process under reduced pressure to obtain the catalyst precursor which is expressed as Co–PPy–TsOH/C. This precursor was pyrolyzed in argon atmosphere at 800 °C for 2 h to obtain the pyrolyzed catalyst of (Co–PPy–TsOH/C)$_P$.

In order to remove the possible metallic cobalt and/or its oxide on the carbon support surface of the (Co–PPy–TsOH/C)$_P$ catalyst produced in the pyrolysis step, the catalyst was treated with 0.5 M H_2SO_4 solution at 90 °C for 4 h and then washed thoroughly with DI water. The resulting catalyst was referred to as (Co–PPy–TsOH/C)$_{P–A}$ (here the subscripted "A" indicates acid treatment). After the acid treatment, the (Co–PPy–TsOH/C)$_{P–A}$ catalyst was further heat-treated in argon atmosphere under 800 °C for 2 h to obtain the catalyst expressed as (Co–PPy–TsOH/C)$_{P–A–P}$.

For comparison, the sample material without Co (expressed as (PPy–TsOH/C)$_P$) and that without PPy–TsOH (expressed as (Co/C)$_P$) were also prepared with the same procedure as described above.

To investigate the effects of cobalt loading on ORR catalytic activity of the (Co–PPy–TsOH/C)$_p$ catalyst, various amounts of $Co(Ac)_2 \cdot 4H_2O$ (0.00625 g, 0.0125 g, 0.025 g, 0.05 g, 0.125 g and 0.25 g) were used to deposit onto 0.5 g of PPy–TsOH/C to form Co–PPy–TsOH/C precursors, followed by pyrolysis in argon at 800 °C for 2 h to obtain catalysts containing different levels of Co loading. The obtained catalysts were expressed as (x-Co–PPy–TsOH/C)$_P$ where x represents the designed cobalt content in the catalyst and the values were 0.25 wt%, 0.5 wt%, 1 wt%, 2 wt%, 5 wt% and 10 wt%, respectively.

To verify the cobalt loading effect, a method of impregnation was used for catalyst synthesis. Specifically, 0.5 g of PPy–TsOH/C was dispersed in a saturated solution of cobalt acetate in 100 ml of DI water. The obtained suspension was refluxed at 60 °C for 10 h. After cooling down to room temperature, the product was collected by filtration, washed thoroughly with ethanol and water, and dried under a vacuum at 45 °C for 12 h to give the powders of (Co–PPy–TsOH/C)$_I$, which was then pyrolyzed in argon atmosphere at 800 °C for 2 h to obtain the catalyst of (Co–PPy–TsOH/C)$_{I–P}$ (here the subscripted "I" indicates the impregnation process).

2.2. Physical characterization

To characterize the crystal structures, XRD patterns of the synthesized catalysts were obtained on a Shimadzu 6000 X-ray diffractometer using Cu K_α radiation ($\lambda = 1.5406$ Å). TEM images taken by a JEOL JEM-2100 instrument operated at 200 kV and 30 mA were used to observe the catalyst powders' morphologies. To identify the possible catalyst active sites, XPS measurements were performed with Kratos AXIS ULTRA DLD with Al K_α as excitation source ($h\nu = 14$ kV). The data were analyzed and sub-peak fitted with the software of XPS Peak 4.1. The cobalt content in the catalysts was detected using a Thermal iCAP 6000 ICP spectrometer by soaking the catalyst in aqua regia.

2.3. Electrochemical evaluation

The electrochemical activity of the catalysts towards ORR was evaluated in a conventional three-electrode cell containing a

working electrode (a rotating disk glassy carbon electrode (RDE) coated by the catalyst), a counter electrode (a platinum wire) and a reference electrode (a saturated calomel electrode, SCE). In the fabricating of working electrode catalyst layer, the catalyst ink was prepared by putting both 6.0 mg of the catalyst powder and 50 μl of Nafion® solution (5 wt%, DuPont) into 950 μl of DI water under ultrasonication to form a suspension ink. Then, 10 μl of this catalyst ink was added onto a pretreated smooth glassy carbon electrode and then air-dried at room temperature to form the catalyst layer. Cyclic voltammograms of the rotating working electrode were recorded between −0.2 and 0.8 V *vs*. SCE (corresponding to 0.04 and 1.04 V *vs*. normal hydrogen electrode, NHE) in either Ar- or O_2-saturated 0.5 M H_2SO_4 solution at 18 °C with a potential scanning rate of 5 mV s^{-1}. The current–voltage curves were carried out at various electrode rotating rates controlled by a Model 636 RDE system (Pine instrument).

The electrochemical measurements were performed using a CHI 750A electrochemical potentiostat/galvanostat, and all electrode potentials reported in the following contents are referenced to NHE except specially stated.

3. Results and discussion

3.1. Physicochemical characterization

Fig. 1 shows the XRD patterns of the synthesized catalyst samples. The two broad diffraction peaks at 2θ of about 25° and 43° for the sample of $(PPy–TsOH/C)_P$ can be assigned to the planes of (002) and (101) of graphitic carbon, respectively. The diffraction profile of the $(Co/C)_P$ sample matches both the JCPDS (PDF-89-4307) and JCPDS (PDF-43-1004) files, indicating the coexistence of metallic α-Co and CoO. Similarly, both metallic cobalt and the Co oxide can also be found in the sample of $(Co–PPy–TsOH/C)_P$ in addition to the graphitic carbon. However, after the acid washing, both of the metallic cobalt and cobalt oxide disappear, as shown in the pattern of $(Co–PPy–TsOH/C)_{P–A}$ sample, indicating that the metallic cobalt and the cobalt oxide have been removed from $(Co–PPy–TsOH/C)_P$ by the acid washing process. There is no visible change in the XRD pattern of the acid-washed $(Co–PPy–TsOH/C)_{P–A}$ sample as shown by $(Co–PPy–TsOH/C)_{P–A–P}$ obtained after a second pyrolysis process, suggesting that this second pyrolysis could not produce additional metal Co and Co oxide.

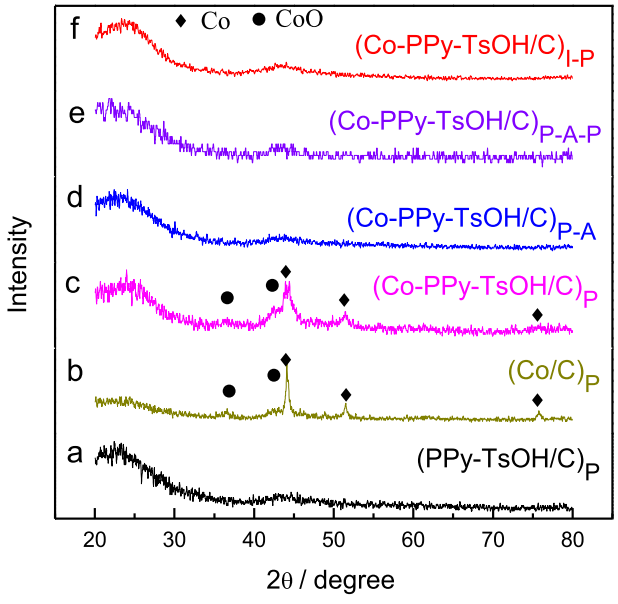

Fig. 1. XRD patterns of the $(PPy–TsOH/C)_P$ (a), $(Co/C)_P$ (b), $(Co–PPy–TsOH/C)_P$ (c), $(Co–PPy–TsOH/C)_{P–A}$ (d), $(Co–PPy–TsOH/C)_{P–A–P}$ (e) and $(Co–PPy–TsOH/C)_{I–P}$ (f) catalysts.

To explore the morphology of the catalysts, TEM images were captured and the obtained results are shown in Fig. 2 for $(Co–PPy–TsOH/C)_P$ (a and b), $(Co–PPy–TsOH/C)_{P–A}$ (c), and $(Co–PPy–TsOH/C)_{P–A–P}$ (d), respectively. The cobalt particles including metallic cobalt and cobalt oxide with a diameter of about 20 nm can be clearly observed in the sample of $(Co–PPy–TsOH/C)_P$ along with an obvious boundary between the carbon support and the cobalt particles as marked therein, indicating that the cobalt particles have been deposited on the carbon surface. Obviously, these metallic Co and Co oxide were formed by the high temperature pyrolysis. In Fig. 2c and d, however, no cobalt particles could be seen in the sample after acid washing or a second pyrolysis, implying that the acid washing has efficiently removed the cobalt particles on the surface of the catalysts. This agrees well with the results of XRD analysis discussed above.

Fig. 3 shows the TEM images of the $(Co–PPy–TsOH/C)_P$ samples with various cobalt loadings. The cobalt particles could be observed in the samples with cobalt loadings higher than 2 wt%, and the amount of the cobalt particles increases with increasing cobalt loading. However, for the samples with cobalt loadings less than 1 wt%, no cobalt particles could be clearly observed, indicating that the cobalt in the $(Co–PPy–TsOH/C)_P$ with Co loading less than 1 wt % may have other existing forms. Based on the results obtained in our previous study, where $Co–N_x$ structure was proved to exist in the $(Co–PPy–TsOH/C)_P$ sample synthesized with APS as oxidant for pyrrole polymerization and cobalt acetate as the metal precursor, [30] we believe that the cobalt in the $(Co–PPy–TsOH/C)_P$ sample with a cobalt loading less than 1 wt% should exist in a form of $Co–N_x$ structure, while both $Co–N_x$ bond and cobalt particles should co-exist when the cobalt loading is higher than 1 wt%. After the Co loading is higher than the coordination capability of the nitrogen in PPy–TsOH, the excessive cobalt would be easily pyrolyzed into metallic cobalt and/or cobalt oxide.

The surface concentrations of cobalt-related species in the samples of $(Co–PPy–TsOH/C)_P$, $(Co–PPy–TsOH/C)_{P–A}$ and $(Co–PPy–TsOH/C)_{P–A–P}$ were also evaluated with XPS analysis, and the Co contents of 0.47 at%, 0.27 at% and 0.32 at%, respectively, were obtained, as listed in Table 1. Compared to the cobalt content of 0.47% in the sample of $(Co–PPy–TsOH/C)_P$ without acid washing, the contents in the other two samples are less but not totally disappeared, implying that the surface cobalt can only be partly removed by the acid washing. This result further confirms the discussion based on both XRD data and TEM images that cobalt in the $(Co–PPy–TsOH/C)_P$ sample can exist as both insoluble portion such as $Co–N_x$ and soluble cobalt particles. In other words, the acid washing can only remove/dissolve the cobalt in the forms of metal and oxide, but could not remove the cobalt bonded with nitrogen in the catalyst. The residual cobalt in the catalysts after acid washing and a second heat treatment are believed to be in the form with a $Co–N_x$ structure.

3.2. Electrochemical characterizations

Fig. 4 shows the background corrected RDE polarization curves for oxygen reduction on the catalyst samples in an O_2-saturated 0.5 M H_2SO_4 solution at a potential scanning rate of 5 mV s^{-1} and an electrode rotating rate of 900 rpm. It can be seen that the $(Co/C)_P$ and $(PPy–TsOH/C)_P$ catalysts have the similar ORR onset potentials, and their ORR catalytic activities are very low although the latter has a higher diffusion current. When cobalt is introduced into $(PPy–TsOH/C)_P$, a substantial increase in the ORR activity as well as the ORR onset potential could be achieved, as observed by (Co–PPy–TsOH/

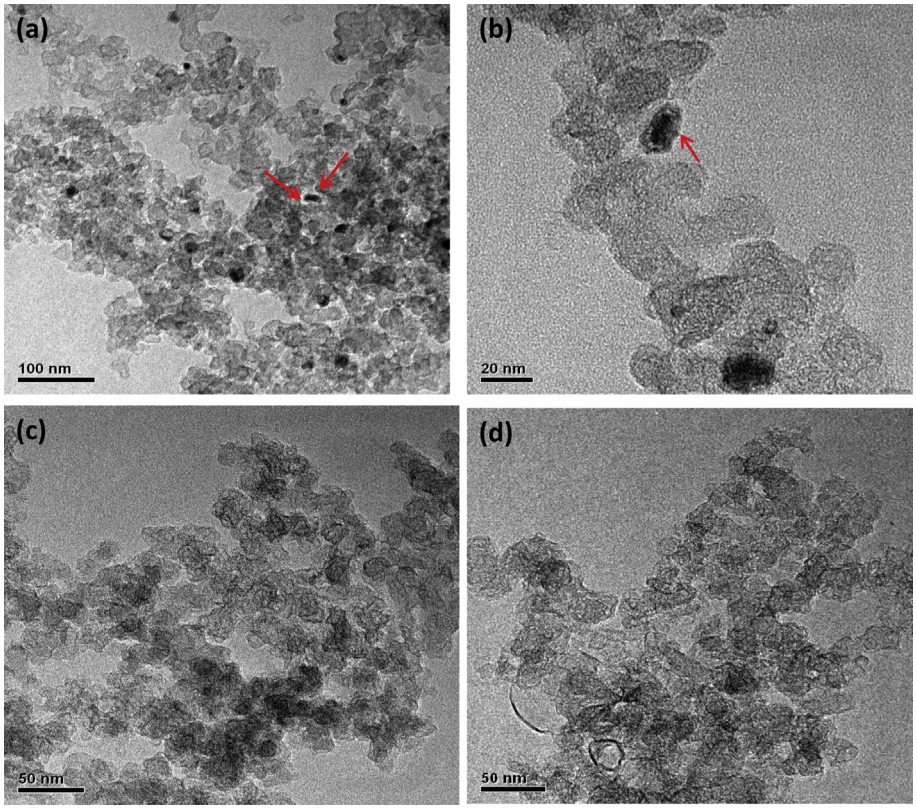

Fig. 2. TEM images of the (Co–PPy–TsOH/C)$_P$ (a&b), (Co–PPy–TsOH/C)$_{P–A}$ (c) and (Co–PPy–TsOH/C)$_{P–A–P}$ (d) catalysts.

C)$_P$ catalyst. Note that the un-pyrolyzed Co–PPy–TsOH/C sample exhibits a much lower ORR activity than that of (Co–PPy–TsOH/C)$_P$, demonstrating the enhancement effect of pyrolysis. Furthermore, the ORR activity of un-pyrolyzed Co–PPy–TsOH/C sample is even worse than those of both (PPy–TsOH/C)$_P$ and (Co/C)$_P$. Comparing the ORR polarization curves of (Co–PPy–TsOH/C)$_P$, (Co–PPy–TsOH/C)$_{P–A}$ and (Co–PPy–TsOH/C)$_{P–A–P}$ as shown in Fig. 4, it can be seen that both the ORR onset potential and the diffusion current are decreased significantly by acid washing. However, after a second pyrolysis, the ORR onset potential of the (Co–PPy–TsOH/C)$_{P–A–P}$

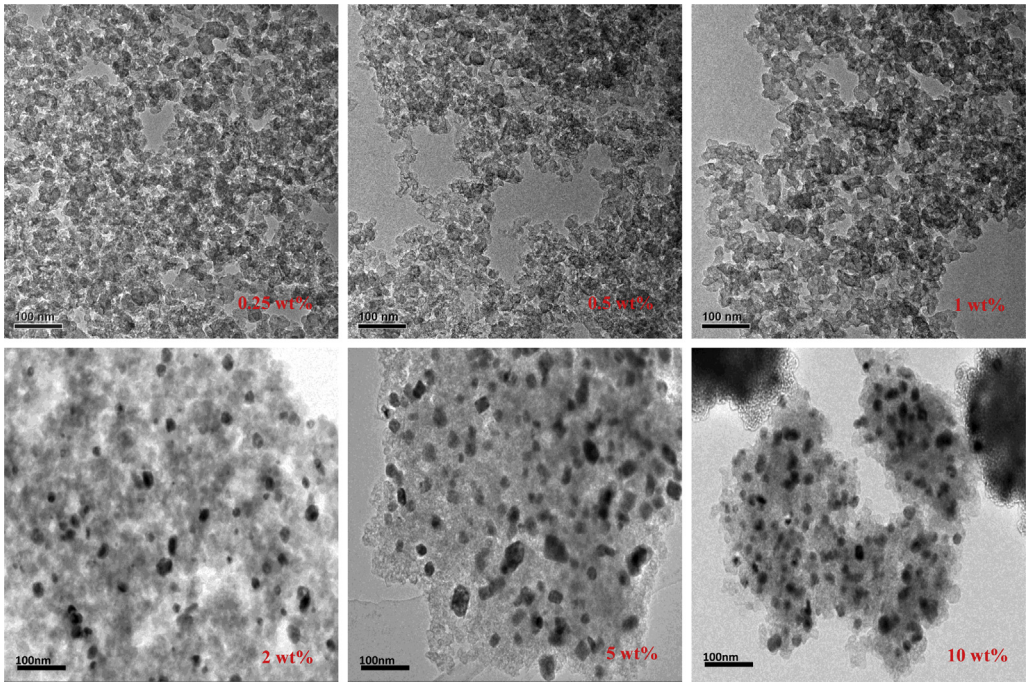

Fig. 3. TEM images of the (x-Co–PPy–TsOH/C)$_P$ catalysts with various cobalt loadings.

Table 1
Surface concentration of Co, N and N 1s peak parameters in the catalyst samples of: I) PPy–TsOH/C; II) $(PPy–TsOH/C)_P$; III) Co–PPy–TsOH/C; IV) $(Co–PPy–TsOH/C)_P$; V) $(Co–PPy–TsOH/C)_{P–A}$; VI) $(Co–PPy–TsOH/C)_{P–A–P}$. Note that there is pyridinic-N-H^+ which could not be distinguished from quaternary-N.

Catalyst sample		I	II	III	IV	V	VI
Total Co content (at.%)		–	–	0.57	0.47	0.27	0.32
Total N content (at.%)		5.06	3.46	4.54	2.44	2.65	2.43
Pyridinic-N (N1)	B.E. (eV)	398.50	398.51	398.81	398.64	398.67	398.69
	Concentration (at.%)	0.131	0.261	0.129	0.333	0.216	0.333
Pyrollic-N (N2)	B.E.(eV)	400.21	400.30	400.26	400.10	400.00	400.25
	Concentration (at.%)	0.678	0.199	0.697	0.208	0.202	0.176
Quaterary-N or Pyridinic-N-H+ (N3)	B.E.(eV)	401.50	401.18	401.60	401.10	401.33	401.20
	Concentration (at.%)	0.190	0.268	0.173	0.240	0.362	0.277
Oxidative-N (N4)	B.E.(eV)	403.00	402.18	403.00	402.30	403.00	402.40
	Concentration (at.%)	0.001	0.272	0.001	0.219	0.220	0.213

catalyst is recovered to the level of $(Co–PPy–TsOH/C)_P$ and the diffusion current is even higher than that of $(Co–PPy–TsOH/C)_P$, further confirming that the pyrolysis process is a necessary step in improving the catalytic ORR activity.

To evaluate the effects of cobalt loading on the ORR activity, Fig. 5 gives the CV curves of the $(x\text{-}Co–PPy–TsOH/C)_P$ catalysts in O_2-saturated 0.5 M H_2SO_4 solution obtained at a potential scanning rate of 5 mV s^{-1}. Normally, the ORR peak potentials, which are listed in Table 2, can be used as the indication to evaluate the catalytic activity of the catalyst. It can be seen that the ORR peak potential increases with increasing cobalt loading and reaches a maximum of 0.712 V at a cobalt loading of 1 wt%. When the cobalt loading is higher than 1 wt%, however, the ORR peak potential decreases with further increasing cobalt loading. This implies that the catalyst of (1.0 wt%-Co–PPy–$TsOH/C)_P$ is the optimal to give the highest ORR catalytic activity.

To quantitatively investigate the Co loading effect on the ORR activity, Fig. 6 gives the RDE curves of the $(x\text{-}Co–PPy–TsOH/C)_P$ catalysts measured at various electrode rotating rates such as 100, 300, 600, 1000 and 1500 rpm, respectively. Generally, the number of electrons exchanged (n) during ORR can be calculated through the Koutecky–Levich (K–L) plots, namely j^{-1} *vs.* $\omega^{-1/2}$, plots: [31]

$$j^{-1} = j_k^{-1} + j_{dl}^{-1} = j_k^{-1} + \left(Bw^{1/2}\right)^{-1} \quad (1)$$

$$B = 0.62nFC_0D_0^{2/3}v_0^{-1/6} \quad (2)$$

where j is the disk current density, j_k is the kinetic current density, j_{dl} is the diffusion current density, F is the Faraday constant, C_0 is the concentration of O_2 in the electrolyte, D_0 is the diffusion coefficient of O_2 in the electrolyte, v_0 is the kinetic viscosity of the electrolyte, and ω is the rotating rate of the disk electrode.

As shown in Fig. 7, the K–L plots were made for the $(x\text{-}Co–PPy–TsOH/C)_P$ catalysts using the current densities at 0.3, 0.4, 0.5 and 0.6 V, respectively, using the RDE data in Fig. 6. All the plots give straight lines with a correlation coefficient larger than 0.99. The electron-transfer numbers of the $(x\text{-}Co–PPy–TsOH/C)_P$ catalysts derived from the K–L plot slopes are listed in Table 2. It can be seen that all the $(x\text{-}Co–PPy–TsOH/C)_P$ catalysts show electron-transfer number close to 4, indicating that 4-electron pathway of the catalyzed ORR is dominating. Similar to the cobalt loading dependence of ORR peak potential discussed in Fig. 5 and Table 2, the electron-transfer number during ORR catalyzed by the $(x\text{-}Co–PPy–TsOH/C)_P$ catalysts increases with increasing cobalt loading to the largest at 1 wt% and then decreases with further increasing cobalt loading, suggesting that the highest selectivity to four-electron-transfer ORR of the $(1.0wt\%\text{-}Co–PPy–TsOH/C)_P$ catalyst. Therefore, it could be concluded that the $(Co–PPy–TsOH/C)_P$ catalyst with a cobalt loading of 1.0 wt% has the best ORR catalytic performance judging from both the activity and four-electron-transfer selectivity.

3.3. Characterization of nitrogen functional groups in the catalysts

There is no doubt that the nitrogen plays a very important role on the ORR catalytic activity of the catalyst. In order to explore the

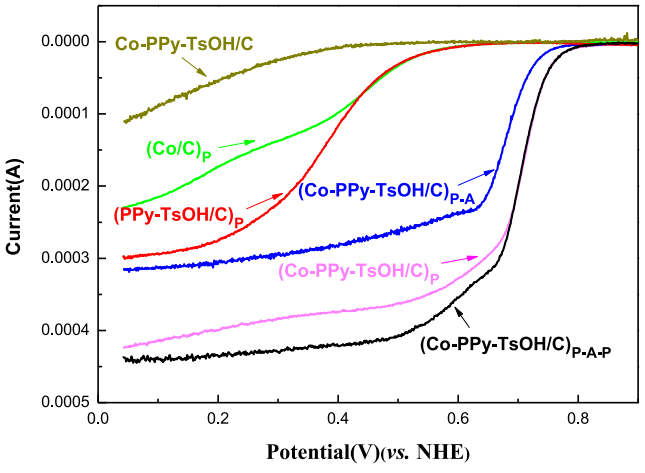

Fig. 4. RDE polarization curves for oxygen reduction on the Co–PPy–TsOH/C, $(Co/C)_P$, $(PPy–TsOH/C)_P$, $(Co–PPy–TsOH/C)_P$, $(Co–PPy–TsOH/C)_{P–A}$ and $(Co–PPy–TsOH/C)_{P–A–P}$ catalysts in O_2-saturated 0.5 M H_2SO_4. Potential scanning rate: 5 mV s^{-1}; electrode rotating rate: 900 rpm.

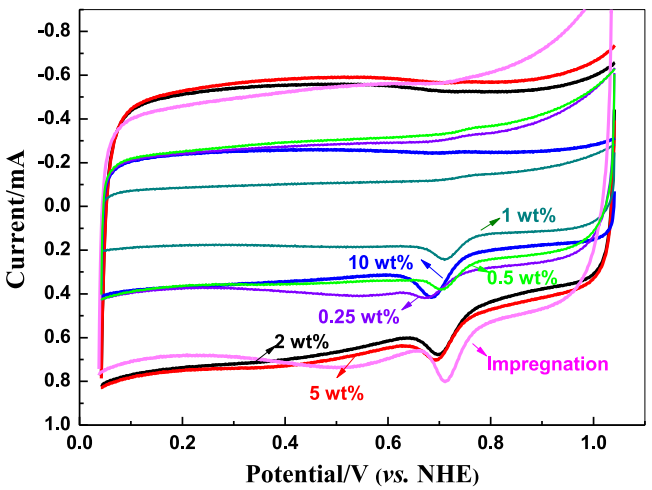

Fig. 5. Cyclic voltammograms for oxygen reduction on the $(x\text{-}Co–PPy–TsOH/C)_P$ and $(Co–PPy–TsOH/C)_{I–P}$ catalysts in O_2-saturated 0.5 M H_2SO_4 solution. Potential scanning rate: 5 mV s^{-1}.

Table 2
ORR peak potential and electron transfer number (n) of the (x-Co–PPy-TsOH/C)$_P$ catalysts.

Co loading	Peak potential (V *vs.* NHE)	Electron transfer number (n)
0.25 wt%	0.673	3.90
0.5 wt%	0.705	3.91
1.0 wt%	0.712	3.94
2.0 wt%	0.698	3.90
5.0 wt%	0.692	3.86
10.0 wt%	0.686	3.82

contribution of various nitrogen functional groups on the ORR activity, the N 1s core level spectra in the samples of PPy–TsOH/C, (PPy–TsOH/C)$_P$, Co–PPy–TsOH/C, (Co–PPy–TsOH/C)$_P$, (Co–PPy–TsOH/C)$_{P-A}$ and (Co–PPy–TsOH/C)$_{P-A-P}$ were captured using XPS, as shown in Fig. 8 and the estimated surface concentrations of nitrogen in total as well as various types of nitrogen in the catalysts are listed in Table 1. It can be seen that the nitrogen concentration decreases form 5.06% in PPy–TsOH/C to 3.46% in (PPy–TsOH/C)$_P$ after the pyrolysis. Similarly, it decreases from 4.54% in Co–PPy–TsOH/C to 2.44% in (Co–PPy–TsOH/C)$_P$. This is probably because of the fact that the pyrrole ring has decomposed at temperature higher than 600 °C and part of the nitrogen in the pyrrole ring has run off during the high temperature pyrolysis [32]. However, the change of nitrogen concentration during the second pyrolysis process from (Co–PPy–TsOH/C)$_{P-A}$ to (Co–PPy–TsOH/C)$_{P-A-P}$ is negligible compared to that during the first pyrolysis from Co–PPy–TsOH/C to (Co–PPy–TsOH/C)$_P$. This implies that the nitrogen atoms might be converted from the N-bonded carbon structure into an in-plane functional group and stabilized due to its incorporation into carbon layer during the first high temperature pyrolysis.

In Fig. 8, the N 1s XPS spectra in various catalysts are deconvoluted into four peaks corresponding to different types of nitrogen: pyridinic-N (N1, 398.0–399.5 eV), pyrrolic-N (N2, 400.1–400.9 eV), quaternary-N (N3, 401–402 eV) and oxidative-N (N4, 402–410 eV). The estimated contents of each type of nitrogen are listed in Table 1. It is apparent that the distribution of surface nitrogen in both PPy–TsOH/C and Co–PPy–TsOH/C could be significantly changed by the pyrolysis. The N 1s spectra in PPy–TsOH/C and Co–PPy–TsOH/C are dominated by a main peak (N2) at 400.25 eV and 400.13 eV, respectively, assigned to the nitrogen atoms in polypyrrole. However, the majority of nitrogen atoms are in the forms of pyridinic-N, quaternary-N and oxidative-N after the pyrolysis, resulted from the decomposition of polypyrrole. This may agree with the observation by Yeager [33] and Wiesener [34] on the M–N/C catalysts created by pyrolyzing macrocyclic compounds. In their study, the transition metals were believed to improve the ORR electrocatalytic activity by facilitating the stable incorporation of nitrogen into the graphitic carbon during the high temperature pyrolysis. In the present work, it can be seen from the deconvoluted results in Table 1 that the nitrogen content in (PPy–TsOH/C)$_P$ is obviously larger than that in (Co–PPy–TsOH/C)$_P$, but the concentration of pyridinic-N in the latter (0.333 at%) is much more than that in the former (0.261 at%), implying that cobalt can facilitate and stabilize the incorporation of pyridinic-N into the graphitic carbon during high temperature pyrolysis, while no similar facilitation can be observed for other types of nitrogen.

According to the study by Liu et al. [19] on Fe–N/C catalyst synthesized with polyacrylonitrile as nitrogen source and iron acetate as the metal precursor, the pyridinic-N in the catalyst could absorb H^+ and then become pyridinic-N–H^+ which is ORR inactive [6,35] when the catalyst was leached with acid solution. However, within the accuracy of XPS measurement, pyridinic-N–H^+ could not be distinguished from quaternary-N. This may give an explanation for the significant decrease of the ORR activity of (Co–PPy–TsOH/C)$_{P-A}$ from that of the unleached catalyst of (Co–PPy–TsOH/C)$_P$, since it is evidently shown in Table 1 that the decrease in N1 content is accompanied with the increase in N3 after the acid washing. After a second pyrolysis, however, the nitrogen content and the content of pyridinic-N could be recovered to the values in the (Co–PPy–TsOH/C)$_P$ catalyst and the XPS spectra was nearly the same as that of (Co–PPy–TsOH/C)$_P$, indicating that the pyridinic-N–H^+ might be changed into pyridinic-N during the second pyrolysis. Since the ORR catalytic properties remained almost unchanged after the second pyrolysis of the acid-washed sample, the recovery of pyridinic-N might play a very important role on the enhancement of ORR activity.

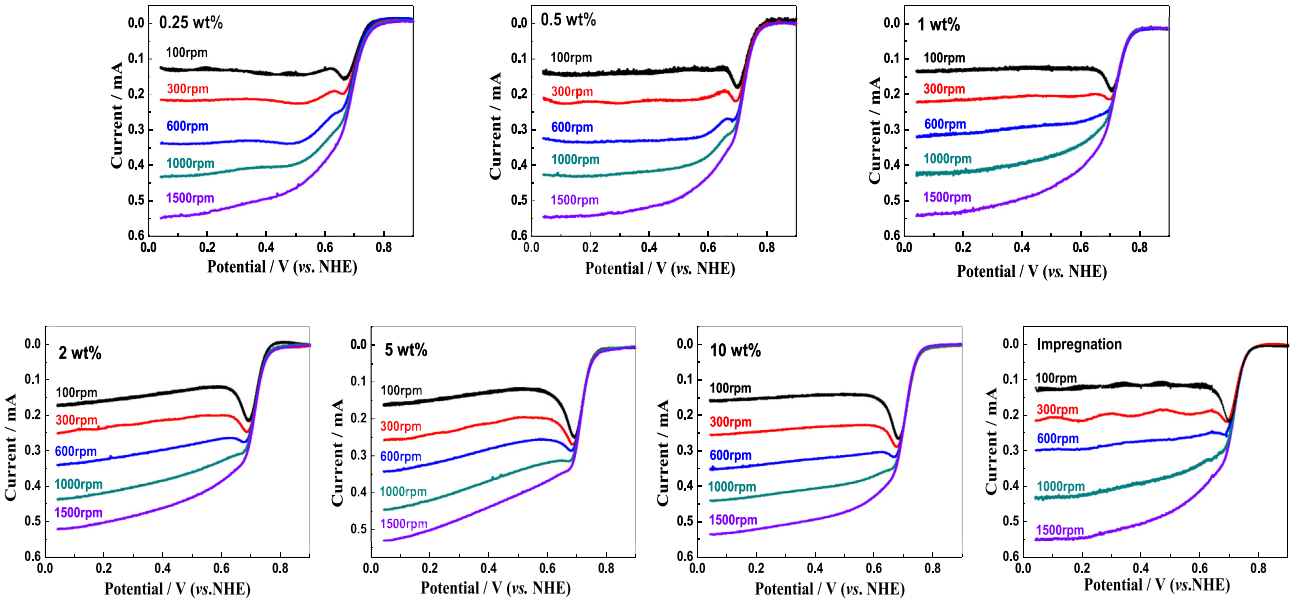

Fig. 6. RDE polarization curves for oxygen reduction on the (x-Co–PPy–TsOH/C)$_P$ and (Co–PPy–TsOH/C)$_{I-P}$ catalysts in O_2-saturated 0.5 M H_2SO_4 solution. Potential scanning rate: 5 mV s^{-1}; electrode rotating rate: 100–1500 rpm.

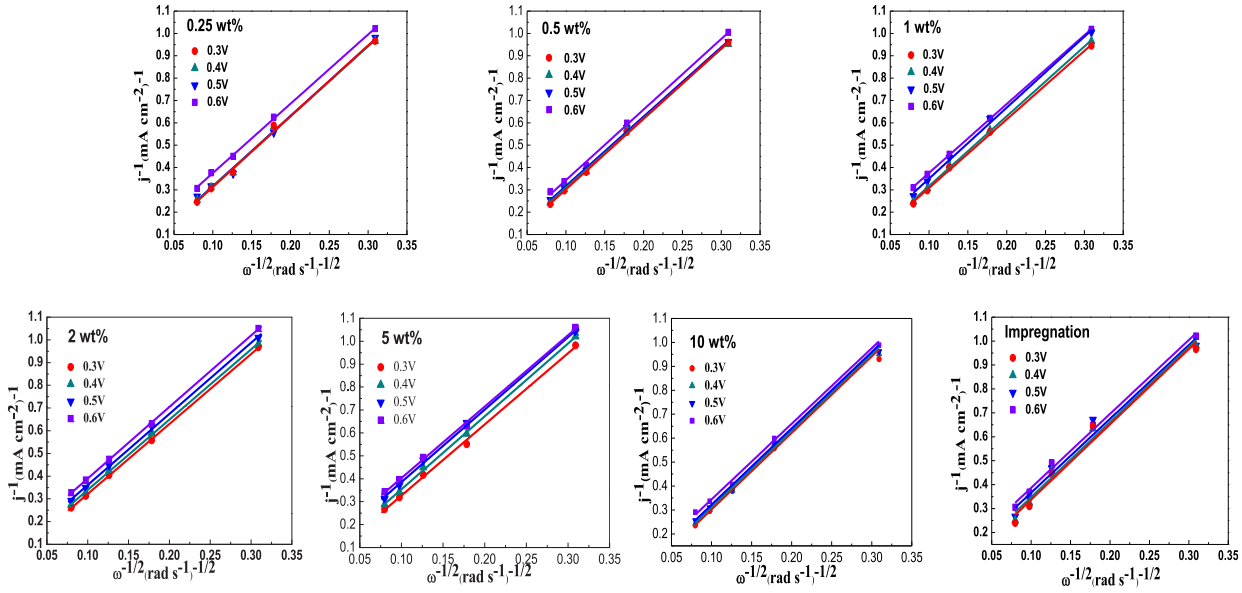

Fig. 7. Koutecky–Levich plots of the (x-Co–PPy–TsOH/C)$_P$ and (Co–PPy–TsOH/C)$_{I-P}$ catalysts obtained with the RDE data shown in Fig. 6.

3.4. Discussion on the ORR active sites

Based on the analysis on N 1s XPS spectra discussed above, it can be seen that the nitrogen in the PPy–TsOH/C catalyst without cobalt could also be inserted into the carbon layer, forming both pyridinic-N and quaternary-N during the pyrolysis which have been believed to be responsible for ORR enhancement [22–25]. However, the poor ORR catalytic activity of (PPy–TsOH/C)$_P$ as shown in Fig. 4 indicates that the residual nitrogen itself cannot enhance the ORR activity, while the significant improvement in ORR activity caused by introducing cobalt to form the catalyst of (Co–PPy–TsOH/C)$_P$ implies that cobalt plays an important role on the enhancement of ORR activity.

For the catalyst of (Co/C)$_P$, cobalt particles including metallic cobalt and cobalt oxide could be deposited on the surface of carbon support (Fig. 1) resulted from the thermal-decomposition of cobalt acetate. The resulting sample had no significant catalytic ORR activity as shown in Fig. 4, implying that neither metallic cobalt nor cobalt oxide is active towards oxygen reduction reaction. However, for the (Co–PPy–TsOH/C)$_P$ catalyst, its metallic Co and Co oxides could be removed after the acid washing, and the resulting sample showed a much less ORR activity than that unwashed sample, as shown in Fig. 4. This seems that its metallic Co and Co oxides might play some roles in ORR activity. But, when this (Co–PPy–TsOH/C)$_{P-A}$ sample was pyrolyzed for the second time, the resulting catalyst ((Co–PPy–TsOH/C)$_{P-A-P}$) did not contain metallic Co and Co oxide as seen in Fig. 1, and the ORR activity was recovered, suggesting that both metallic Co and Co oxide might not play a role in ORR activity. Therefore, the ORR active sites in the (Co–PPy–TsOH/C)$_P$ catalysts should have a Co–N structure, as generally believed. Recalling the effects of cobalt loading on the ORR catalytic activity of the (x-Co–PPy–TsOH/C)$_P$ catalysts discussed above, it is believed that a cobalt loading of 1.0 wt% should be the balancing point to synthesize the catalyst with cobalt in the form of only Co–N_x structure without metallic cobalt and Co oxide particles, which could give the optimal ORR activity. When the cobalt loading is larger than 1.0 wt%, however, both Co–N_x structure and cobalt particles exist in the catalyst and the latter may cover some of the Co–N_x active sites, leading to a decreased ORR activity. The more the cobalt loading, the more cobalt particles are produced in the catalyst, and the more active sites would be covered, resulting in the reduced ORR activity. On the other hand, when the cobalt loading is lower than 1.0 wt%, there is not enough cobalt to bond with nitrogen to form the active sites, leading to a decreased ORR activity. The less the cobalt loading, the less the Co–N_x ORR active sites could be produced, resulting in a lower ORR activity.

To verify this opinion, another catalyst of (Co–PPy–TsOH/C)$_{I-P}$ was prepared by an impregnation method as described in the experimental section. The main difference between the catalysts of (Co–PPy–TsOH/C)$_P$ and (Co–PPy–TsOH/C)$_{I-P}$ is that: for (Co–PPy–TsOH/C)$_{I-P}$, only the cobalt bonded to PPy in PPy–TsOH/C exists in the final catalyst, the excessive cobalt that unbonded to PPy is thoroughly washed by filtration. For this (Co–PPy–TsOH/C)$_{I-P}$ sample, XRD measurement confirmed that neither metallic cobalt nor cobalt oxide existed in the sample (Fig. 1), and the Co loading in such a (Co–PPy–TsOH/C)$_{I-P}$ catalyst was measured using ICP to be 1.16 wt%, which is fairly close to 1.2 wt% of the optimal (1.0 wt%-Co–PPy–TsOH/C)$_P$ catalyst, further supports that all cobalt are bonded to nitrogen to form Co–N active sites in this catalyst. Regarding the catalytic behaviors of (Co–PPy–TsOH/C)$_{I-P}$ and (1.0 wt%-Co–PPy–TsOH/C)$_P$ catalysts, both their CV curves (Fig. 5) and RDE data (Fig. 6) gave almost the same ORR catalytic activity, suggesting that both of these catalysts should have the similar Co-N_x active sites.

To demonstrate the formation of ORR active site in the (Co–PPy–TsOH/C)$_P$ catalyst, a schematic is shown in Fig. 9. When the carbon supported PPy–TsOH is suspended into an aqueous solution of cobalt acetate, PPy–TsOH on the carbon surface can release proton from N–H group on pyrrole ring and then react with cobalt ion to form the Co-pyrrolic-N structure [21,27]. During the followed pyrolysis, the Co-pyrrolic-N structure could be transformed into the Co-pyridinic-N structure which should be the ORR active site in the catalyst. This gives a good explanation to the results described above that the residual nitrogen itself cannot enhance the ORR activity but the Co bonded pyridinic-N plays a very important role in the enhancement of ORR activity while metallic cobalt and cobalt oxide particles deposited on the carbon support are not responsible for the ORR activity. However, because it is not necessary for all the N–H

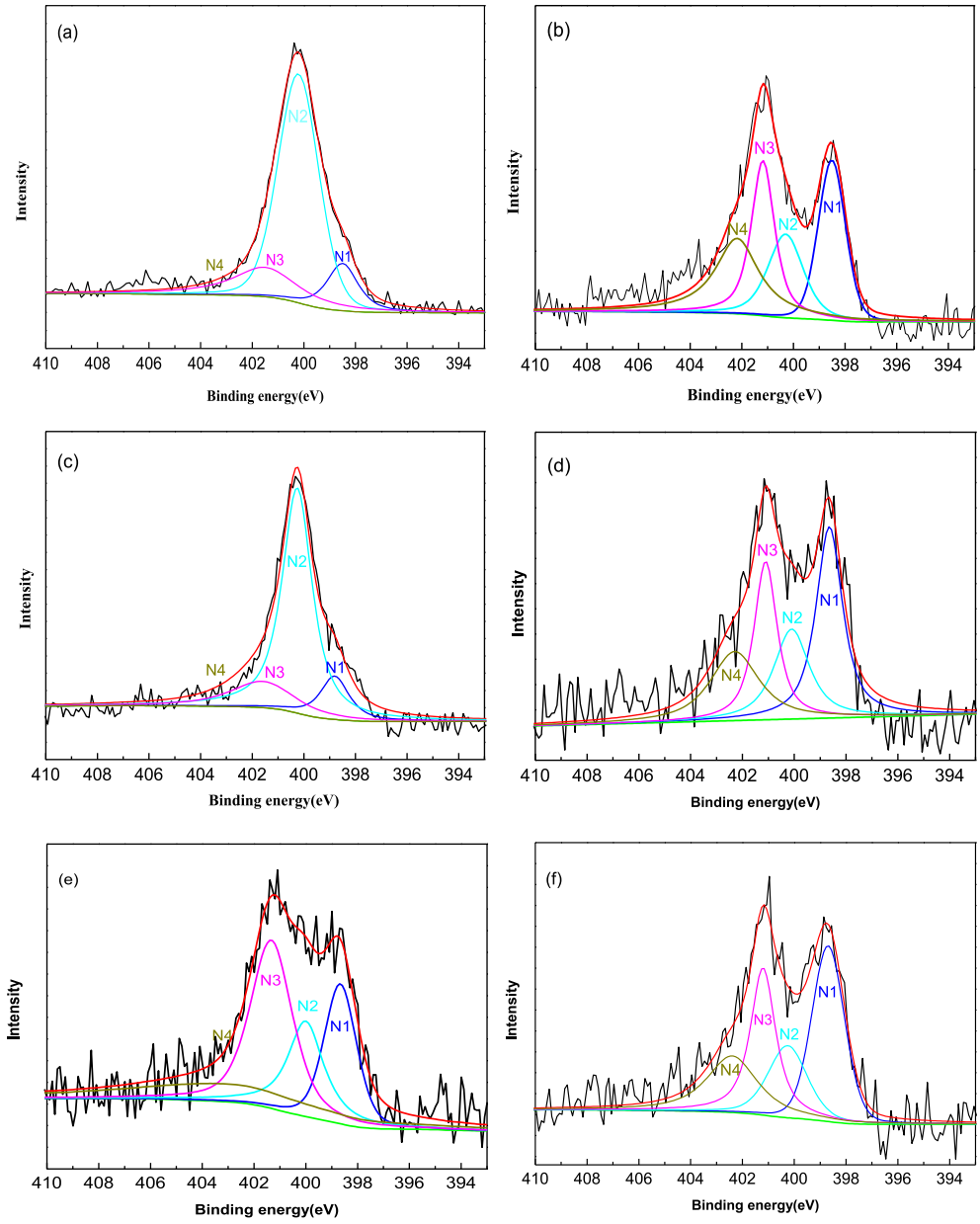

Fig. 8. XPS spectra of N 1s in the PPy-TsOH/C (a), $(PPy-TsOH/C)_P$ (b), Co−PPy−TsOH/C (c), $(Co-PPy-TsOH/C)_P$ (d),$(Co-PPy-TsOH/C)_{P-A}$ (e) and $(Co-PPy-TsOH/C)_{P-A-P}$ (f) catalysts.

groups on pyrrole to release the proton for reacting with cobalt ion, the unbonded nitrogen atoms may change into quaterany-N, oxidative-N and pyridinic-N as well as residual pyrrolic-N inserted into the carbon layer during the pyrolysis. Therefore, all four types of nitrogen can be observed in the final $(Co-PPy-TsOH/C)_P$ catalyst.

4. Conclusions

To identify the possible ORR active sites in the catalyst of $(Co-PPy-TsOH/C)_P$, a series of contrastive catalyst samples were synthesized. Their morphologies/structures and compositions were characterized by XRD, TEM, XPS as well as ICP techniques, and the catalytic activities towards ORR were comparatively investigated and analyzed based on cyclic voltammetric and RDE measurements. Based on the experimental observations, the following conclusions can be made: (1) the cobalt in $(Co-PPy-TsOH/C)_P$ exists in the forms of nitrogen-bonded species ($Co-N_x$) along with metallic cobalt and cobalt oxide, and the relative compositions are strongly dependent on the cobalt loading. When the loading of cobalt is 1.0 wt% or lower, the dominating form of cobalt is $Co-N_x$; when the loading is higher than 1.0 wt%, however, $Co-N_x$, metallic Co and cobalt oxide particles are co-existed in the catalyst; (2) in the cobalt loading range from 0.25 to 1.0 wt%, the ORR activity increases with increasing the cobalt loading and reaches a maximum at ~1.0 wt%, then decreases with further increasing cobalt loading, probably because of a blocking effect of the excessive ORR inactive species such as metallic Co and cobalt oxide particles; (3) the acid washing can only remove the cobalt particles such as metallic Co and cobalt oxide deposited on the carbon support surface, but the Co−N structure still remains in the catalyst after acid washing; (4) both metallic Co and cobalt oxide in $(Co-PPy-TsOH/C)_P$ and the un-bonded N by Co hardly contribute to the ORR activity; and (5) the ORR active site in $(Co-PPy-TsOH/C)_P$ catalyst is likely a Co-pyridinic-N group.

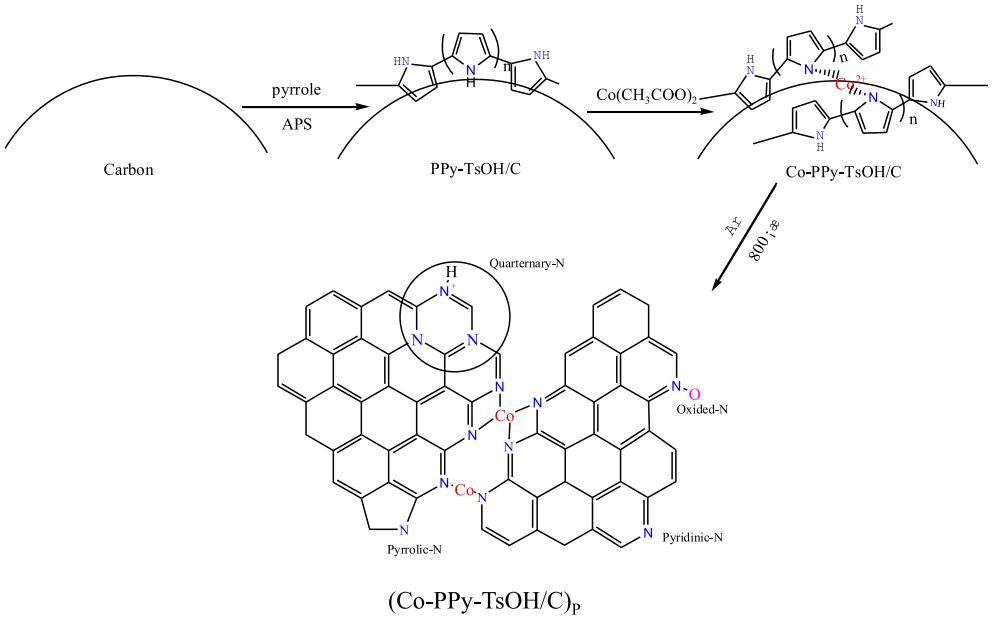

Fig. 9. Schematic representation of the formation of ORR active site in the (Co–PPy–TsOH/C)$_P$ catalyst.

Acknowledgments

The authors are grateful for the financial support of this work by the National Science Foundation of China (21176155) and the STCSM of China (10JC1406900).

References

[1] G. Brumfiel, Nature 422 (2003), 104–104.
[2] R. Bashyam, P. Zelenay, Nature 443 (2006) 63–66.
[3] H.R. Colón-Mercado, B.N. Popov, J. Power Sources 155 (2006) 253–263.
[4] C.W.B. Bezerra, L. Zhang, K. Lee, H. Liu, A.L.B. Marques, E.P. Marques, H. Wang, J. Zhang, Electrochim. Acta 53 (2008) 4937–4951.
[5] G. Faubert, G. Lalande, R. Côté, D. Guay, J.P. Dodelet, L.T. Weng, P. Bertrand, G. Dénès, Electrochim. Acta 41 (1996) 1689–1701.
[6] G. Lalande, R. Côté, G. Tamizhmani, D. Guay, J.P. Dodelet, L. Dignard-Bailey, L.T. Weng, P. Bertrand, Electrochim. Acta 40 (1995) 2635–2646.
[7] M.C.M. Alves, J.P. Dodelet, D. Guay, M. Ladouceur, G. Tourillon, J. Phys. Chem. 96 (1992) 10898–10905.
[8] M. Lefèvre, J.P. Dodelet, P. Bertrand, J. Phys. Chem. B 106 (2002) 8705–8713.
[9] G. Lalande, R. Côté, D. Guay, J.P. Dodelet, L.T. Weng, P. Bertrand, Electrochim. Acta 42 (1997) 1379–1388.
[10] X. Yuan, X. Zeng, H.J. Zhang, Z.F. Ma, C.Y. Wang, J. Am. Chem. Soc. 132 (2010) 1754–1755.
[11] H. Zhong, H. Zhang, Y. Liang, J. Zhang, M. Wang, X. Wang, J. Power Sources 164 (2007) 572–577.
[12] N.A. Vante, H. Tributsch, Nature 323 (1986) 431–432.
[13] A. Lewera, J. Inukai, W.P. Zhou, D. Cao, H.T. Duong, N. Alonso-Vante, A. Wieckowski, Electrochim. Acta 52 (2007) 5759–5765.
[14] D.C. Papageorgopoulos, F. Liu, O. Conrad, Electrochim. Acta 52 (2007) 4982–4986.
[15] F. Jaouen, S. Marcotte, J.P. Dodelet, G. Lindbergh, J. Phys. Chem. B 107 (2003) 1376–1386.
[16] M. Lefèvre, J.P. Dodelet, P. Bertrand, J. Phys. Chem. B 104 (2000) 11238–11247.
[17] K. Lee, L. Zhang, H. Lui, R. Hui, Z. Shi, J. Zhang, Electrochim. Acta 54 (2009) 4704–4711.
[18] J.A.R. van Veen, H.A. Colijn, J.F. van Baar, Electrochim. Acta 33 (1988) 801–804.
[19] G. Liu, X. Li, P. Ganesan, B.N. Popov, Appl. Catal. B-Environ. 93 (2009) 156–165.
[20] M. Chisaka, T. Iijima, Y. Ishihara, Y. Suzuki, R. Inada, Y. Sakurai, Electrochim. Acta 85 (2012) 399–410.
[21] M. Kobayashi, H. Niwa, Y. Harada, K. Horiba, M. Oshima, H. Ofuchi, K. Terakura, T. Ikeda, Y. Koshigoe, J.I. Ozaki, S. Miyata, S. Ueda, Y. Yamashita, H. Yoshikawa, K. Kobayashi, J. Power Sources 196 (2011) 8346–8351.
[22] Y. Shao, J. Sui, G. Yin, Y. Gao, Appl. Catal. B-Environ. 79 (2008) 89–99.
[23] P.H. Matter, L. Zhang, U.S. Ozkan, J. Catal. 239 (2006) 83–96.
[24] T.C. Nagaiah, S. Kundu, M. Bron, M. Muhler, W. Schuhmann, Electrochem. Commun. 12 (2010) 338–341.
[25] J.I. Ozaki, S.I. Tanifuji, N. Kimura, A. Furuichi, A. Oya, Carbon 44 (2006) 1324–1326.
[26] A. Cioffarelli, M.T. Natale, Guide to the Catacombs of Rome and Its Surroundings, English ed., Bonsignori, Rome, 2000, p. 135.
[27] Z.P. Li, Z.X. Liu, K.N. Zhu, Z. Li, B.H. Liu, J. Power Sources 219 (2012) 163–171.
[28] C.W.B. Bezerra, L. Zhang, H. Liu, K. Lee, A.L.B. Marques, E.P. Marques, H. Wang, J. Zhang, J. Power Sources 173 (2007) 891–908.
[29] X. Yuan, X.L. Ding, C.Y. Wang, Z.F. Ma, Energy Environ. Sci. 6 (2013) 1105–1124.
[30] H.D. Sha, X. Yuan, X.X. Hu, H. Lin, W. Wen, Z.F. Ma, J. Electrochem. Soc. 160 (2013) F507–F513.
[31] Y. Hu, X. Zhao, Y. Huang, Q. Li, N.J. Bjerrum, C. Liu, W. Xing, J. Power Sources 225 (2013) 129–136.
[32] J.Z. Wang, S.L. Chou, J. Chen, S.Y. Chew, G.X. Wang, K. Konstantinov, J. Wu, S.X. Dou, H.K. Liu, Electrochem. Commun. 10 (2008) 1781–1784.
[33] E. Yeager, Electrochim. Acta 29 (1984) 1527–1537.
[34] K. Wiesener, Electrochim. Acta 31 (1986) 1073–1078.
[35] T. Okada, M. Gokita, M. Yuasa, I. Sekine, J. Electrochem. Soc. 145 (1998) 815–822.